Generalized Math Model for Simulation of High-Altitude Balloon Systems

N. J. Nigro,* J. K. Yang,† and A. F. Elkouh*
Marquette University, Milwaukee, Wisconsin
and
D. E. Hinton‡
NASA Langley Research Center, Hampton, Virginia

Balloon systems have proved to be a cost-effective means for conducting research experiments (e.g., infrared astronomy) in the Earth's atmosphere. The purpose of this paper is to present a generalized mathematical model that can be used to simulate the motion of these systems once they have attained float altitude. The resulting form of the model is such that the pendulation and spin motions of the system are uncoupled and can be analyzed independently. The model is evaluated by comparing the simulation results with data obtained from an actual balloon system flown by NASA.

Introduction

BALLOON systems similar to the one shown in Fig. 1 are employed extensively as a cost-effective means of conducting various experiments in the Earth's atmosphere.[1] In many of these experiments, it is necessary to stabilize the research platform or determine its orientation (as a function of time) in order to process the experimental data. This can be accomplished with the use of auxiliary control or attitude determination systems. Hence, it is necessary to employ reliable mathematical models for balloon system simulation in order to design the auxiliary systems or determine whether they are actually necessary to process the experimental data within the required precision.

The main purpose of this paper is to present a general mathematical model that can be used to simulate the motion of balloon systems once they have attained equilibrium at float altitude. The model is evaluated by comparing simulation results with data obtained from an actual balloon system flown by NASA. The research reported in this paper is an extension of previous work reported in Refs. 2-8.

System Idealization

The motion of balloon systems (such as the one shown in Fig. 1) is very complex and involves various coupled motions including bounce, horizontal translation, pendulation, and spin. The complexity of the motion increases with the number of connectors used in the system. The development of a mathematical model that can be used to predict this motion is complicated by a number of factors: 1) the balloon subsystem is a flexible (distributed parameter) system with motion in an infinite fluid medium, 2) the system is subjected to wind gusts that are difficult to predict, and 3) the motion of the kinematic joints connecting the links is sometimes difficult to model. The latter is true, for example, in the case of the ring-and-clevis connectors employed in many balloon systems.

The mathematical model for the balloon system is developed by employing the rigid-body dynamic equations that are coupled, through the boundary conditions, with the fluid dynamic equations. The resulting model is very complex and consists of a system of coupled partial and ordinary differential equations. For purposes of this research, the model is simplified by making the following idealizations:

1) The system is treated as a mechanical system comprised of three rigid links connected by idealized spherical joints. The system is lumped as shown in Fig. 2; i.e., the balloon and research platform are treated as rigid-body links with distributed mass, while the interconnecting suspension system is idealized as a link comprised of point masses connected by an inextensible line.

2) The balloon is treated as an equivalent rigid body. The aerodynamic forces and torques, which result from the interaction of the balloon and fluid (air and helium), are treated as external reactions acting on this rigid body.

3) The coupling effect of the suspension system is included by assuming that it has equivalent torsional stiffness, torsional moment of inertia, and torsional damping. The torsional stiffness and damping are functions of the type of joints, the magnitude of the relative spin motion between the balloon and platform, and the torsional properties of the suspension system. Thus, the torsional stiffness is zero for the case of a suspension comprised of rigid links connected by ideal ball-and-socket joints. Clearly, it is difficult to determine these parameters in the case of a suspension system comprised of ring-and-clevis joints or where one of the links consists of a parachute. (See Fig. 1.) The effect of the torsional stiffness and damping in the platform connector (such as the one shown in Fig. 1) are also included in the model.

4) The viscous drag forces acting on the suspension links and research platform are neglected. The viscous drag reactions included in the development of this model are the aerodynamic drag forces acting on the balloon, the aerodynamic drag torque that retards the spin (torsion) of the balloon, and the drag torque that results from torsional damping in the suspension. The drag torque components that arise due to the pendulation of the links are neglected since these are small relative to the gravity torque components. All viscous

Received Sept. 3, 1984; revision received March 15, 1985.

*Professor of Mechanical Engineering.
†Graduate Student.
‡Aero-Space Technologist.

drag forces and torques are linearized in order to facilitate uncoupling of the resulting form of the system model.

5) In general, all velocities, accelerations, and displacements of the balloon system are assumed to be small. The only exceptions to this are the absolute horizontal translational and spin displacements of the system. The relative spin displacements between adjoining links, as well as the variations in the float altitude due to changes in the properties (or losses) of helium, are assumed to be small.

6) External forces acting on the balloon due to the presence of wind gusts are included in this model in order to study their effect on the motion of the system. However, the variation of wind gusts in the spatial directions is neglected.

Kinematics

The configuration of the idealized system shown in Fig. 2 can be prescribed in terms of 12 generalized coordinates. The following generalized coordinates were chosen for this research; i.e., three translational coordinates to locate m_0 at the mass center of the balloon and nine rotational coordinates to prescribe the orientation of the three links. The reference coordinate system is assumed to be an inertial system whose origin coincides with the initial location of m_0 and whose orientation is coincident with the initial orientation of the research platform body axes. In most cases, these initial coordinate values are obtained from radar tracking and from instrumentation (e.g., magnetometers) attached to the research platform.

There are several sets of Euler angles that are possible for fixing the orientation of the links. The set chosen for this research is one that leads to the uncoupling of the math model. The sequence of three rotations (see Fig. 3) that define this set is given as follows: 1) a positive rotation θ_3 about the x_3 axis, 2) a positive rotation θ_2 about the new position of the x_1 (i.e., the x_1') axis, and 3) a positive rotation θ_1 about the x_2'' axis. The angles θ_1 and θ_2 measure pendulation in the $x_1'' x_3''$ and $x_2' x_3'$ planes, respectively, while the angle θ_3 measures spin about the x_3 axis.

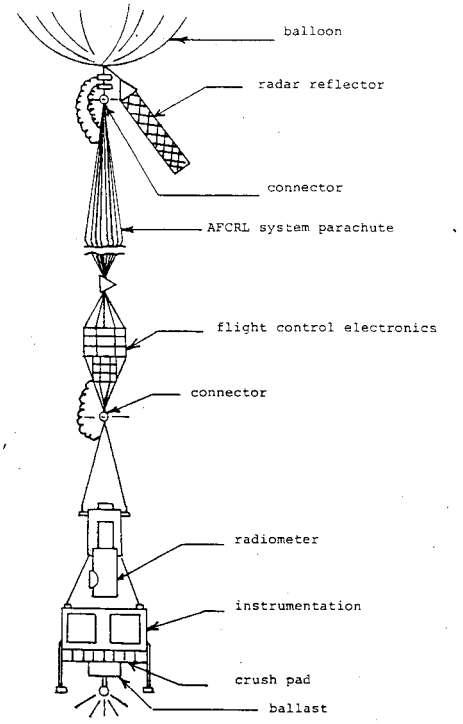

Fig. 1 Balloon system for conducting research in Earth's atmosphere.

The angular velocity $\bar{\omega}^{(i)}$ for the ith ($i=1,2,3$) link is given in terms of the Euler angles and their rates as

$$\bar{\omega}^{(i)} = \omega_1^{(i)} \bar{e}_1^{(i)} + \omega_2^{(i)} \bar{e}_2^{(i)} + \omega_3^{(i)} \bar{e}_3^{(i)}$$

$$\omega_1^{(i)} = -\dot{\theta}_3^{(i)} \sin\theta_1^{(i)} \cos\theta_2^{(i)} + \dot{\theta}_2^{(i)} \cos\theta_1^{(i)}$$

$$\omega_2^{(i)} = \dot{\theta}_3^{(i)} \sin\theta_2^{(i)} + \dot{\theta}_1^{(i)}$$

$$\omega_3^{(i)} = \dot{\theta}_3^{(i)} \cos\theta_2^{(i)} \cos\theta_1^{(i)} + \dot{\theta}_2^{(i)} \sin\theta_1^{(i)} \tag{1}$$

where

$\omega_j^{(i)}$ = component of the angular velocity of the ith link along $x_j^{(i)}$
$\theta_j^{(i)}$ = angle describing orientation of ith link
$x_j^{(i)}$ = jth body axis with origin at m_i
$\bar{e}_j^{(i)}$ = unit vector along $x_j^{(i)}$

Under the assumption of small motion, Eq. (1) simplifies to

$$\omega_1^{(i)} = \dot{\theta}_2^{(i)}, \quad \omega_2^{(i)} = \dot{\theta}_1^{(i)}, \quad \text{and} \quad \omega_3^{(i)} = \dot{\theta}_3^{(i)} \tag{2}$$

The expressions for the components of the translational velocities of m_i ($i=1,2,3$) are given as

$$\bar{v}^{(0)} = \dot{u}_1^{(0)} \bar{e}_1^{(3)} + \dot{u}_2^{(0)} \bar{e}_2^{(3)} + \dot{u}_3^{(0)} \bar{e}_3^{(3)}$$

$$\bar{v}^{(i)} = \left[\dot{u}_1^{(0)} - \sum_{j=1}^{i} r_j \dot{\theta}_1^{(j)}\right] \bar{e}_1^{(3)} + \left[\dot{u}_2^{(0)} + \sum_{j=1}^{i} r_j \dot{\theta}_2^{(j)}\right] \bar{e}_2^{(3)} + \dot{u}_3^{(0)} \bar{e}_3^{(3)} \tag{3}$$

where

$\bar{v}^{(0)}$ = velocity of balloon mass center
$\bar{v}^{(i)}$ = velocity of m_i
$\dot{u}_j^{(0)}$ = component of $\bar{v}^{(0)}$ along $x_j^{(3)}$ axis
r_j = length of the jth link
$\bar{e}_j^{(3)}$ = unit vectors along the body axis is fixed in the research platform with origin at m_3
$x_j^{(0)} = x_j^{(I)}$

Equation (3) was obtained by resolving $\bar{v}^{(i)}$ into components along the research platform body axes and then employing the small-angle approximation. (See idealization 5.)

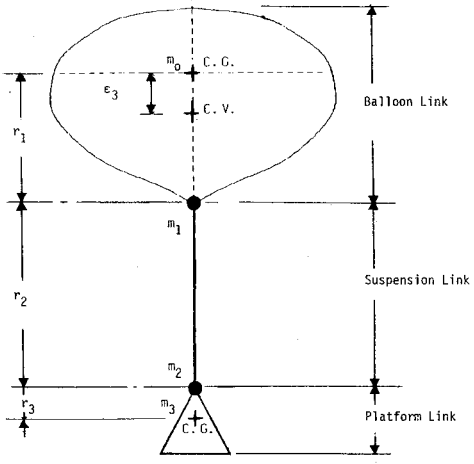

Fig. 2 Idealized balloon system.

Lagrange's Equations

The general form of Lagrange's equation is given as follows; i. e.,

$$\frac{\mathrm{d}}{\mathrm{d}t}\frac{\partial L}{\partial \dot{q}_i}-\frac{\partial L}{\partial q_i}=Q_i,\ (i=1,\ \ldots,n) \tag{4}$$

where n is the number of degrees of freedom, q_i the generalized coordinate, $L=T-V$, T the system kinetic energy, V the potential energy, and Q_i the generalized force associated with q_i.

The kinetic energy T for the generalized balloon system shown in Fig. 2 can be calculated from the following expressions:

$$T=\sum_{i=1}^{3} T^{(i)}$$

$$T^{(1)}=\frac{m_0}{2}[(v_1^{(0)})^2+(v_2^{(0)})^2+(v_3^{(0)})^2]+\frac{1}{2}[I_{11}^{(1)}(\omega_1^{(1)})^2+I_{22}^{(1)}(\omega_2^{(1)})^2+I_{33}^{(1)}(\omega_3^{(1)})^2]+\frac{m_1}{2}[(v_1^{(1)})^2+(v_2^{(1)})^2+(v_3^{(1)})^2]$$

$$T^{(2)}=\frac{m_2}{2}[(v_1^{(2)})^2+(v_2^{(2)})^2+(v_3^{(2)})^2]+\frac{1}{2}I_{33}^{(2)}(\omega_3^{(2)})^2$$

$$T^{(3)}=\frac{m_3}{2}[(v_1^{(3)})^2+(v_2^{(3)})^2+(v_3^{(3)})^2]+\frac{1}{2}[I_{11}^{(3)}(\omega_1^{(3)})^2+I_{22}^{(3)}(\omega_2^{(3)})^2+I_{33}^{(3)}(\omega_3^{(3)})^2] \tag{5}$$

where m_0 is the mass of balloon shell and helium, $I_{ii}^{(j)}$ the principal moment of inertia (of the jth link) with respect to the $x_i^{(j)}$ body axis, and $v_j^{(i)}$ the velocity component of m_i along the $x_j^{(3)}$ axis.

The system potential energy (V) is due to the presence of the static buoyancy and gravity forces. It is given (with respect to a horizontal reference located at m_0) by the following expressions:

$$V=\sum_{i=0}^{3} V^{(i)}$$

$$V^{(0)}=F\,\epsilon_3\cos\theta_1^{(1)}\cos\theta_2^{(1)}+\frac{K^{(0)}[u_3^{(0)}]^2}{2}$$

$$F=\sum_{i=0}^{3} m_i g$$

$$V^{(i)}=[-m_i g]\sum_{j=1}^{i} r_j\cos\theta_1^{(j)}\cos\theta_2^{(j)}$$

$$K^{(0)}=-\frac{V_b g^2\rho_a^2(\eta_h-1)}{\eta_h P_0} \tag{6}$$

where V_b is the volume of balloon, ρ_a the density of air at float altitude, g the acceleration of gravity at float altitude, F the static buoyancy force, $K^{(0)}$ the equivalent spring constant due to small variations in the static buoyancy force at float altitude, P_0 the pressure of air at float altitude, η_h the ratio of specific heats (c_p/c_v) for helium, and ϵ_3 the distance along $x_3^{(1)}$ axis between the center of mass and center of volume of the balloon.

It should be noted that the distance ϵ_3 is zero for a spherical balloon; however, the center of volume is usually located below the center of mass in the case of zero pressure balloons.

Generalized Forces

The generalized forces Q_i stem from the presence of the aerodynamic reactions acting on the balloon and the torsional properties of the suspension system. The aerodynamic reactions included in this development are the dynamic buoyancy forces, inertia drag forces, inertia drag torques, viscous drag forces, and viscous drag torques. Additional generalized forces due to the equivalent torsional stiffness and damping in the suspension system and connectors are also included. A detailed discussion of the aerodynamic reactions can be found in Ref. 2.

The absolute acceleration of the fluid (air) approaching the balloon results in a uniform pressure drop across the balloon in the direction of the acceleration of the fluid. This pressure drop, when integrated over the balloon surface, results in a force that acts on the balloon in the direction of the fluid acceleration. The force acts at the center of buoyancy of the balloon and is termed the dynamic buoyancy force. The expressions for the resulting generalized forces are

$$Q_{u_i}^{B}(0)=\rho_a V_b \dot{w}_i^{(0)}$$

$$Q_{\theta_1}^{B}(1)=\rho_a V_b \epsilon_3 \dot{w}_2^{(0)}$$

$$Q_{\theta_2}^{B}(1)=\rho_a V_b \epsilon_3 \dot{w}_1^{(0)}$$

$$Q_{\theta_3}^{B}(1)=\rho_a V_b[\epsilon_1 \dot{w}_2^{(0)}-\epsilon_2 \dot{w}_1^{(0)}] \tag{7}$$

where Q_{qi}^{B} is the generalized dynamic buoyancy force associated with q_i, $\dot{w}_i^{(0)}$ the component of gust acceleration

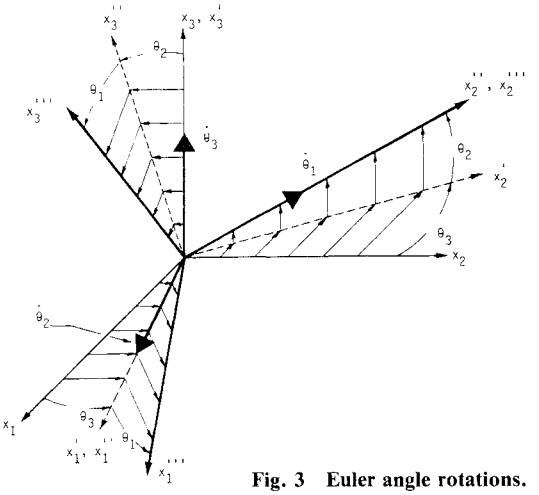

Fig. 3 Euler angle rotations.

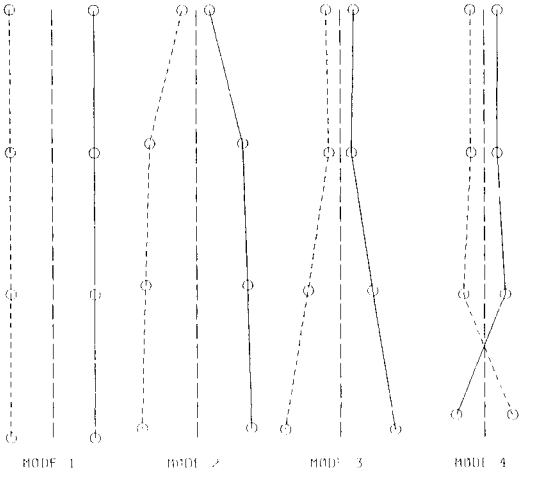

Fig. 4 Modal shapes for LACATE system.

in the $\bar{e}_i^{(3)}$ direction, and ϵ_1, ϵ_2, ϵ_3, the eccentricity components (in $x_j^{(1)}$ direction) of the dynamic buoyancy force measured relative to the balloon center of gravity.

The eccentricity parameters ϵ_1, and ϵ_2 are introduced in Eq. (7) in order to enable designers to study the effect of the external disturbances exciting spinning motion of the balloon system. In this development, it is assumed that the parameter ϵ_3 is much greater than ϵ_1 and ϵ_2. The effect can be eliminated by setting $\epsilon_1 = \epsilon_2 = 0$.

A balloon undergoing translational and angular acceleration in a fluid medium is subjected to resisting forces and torques even if the fluid is nonviscous. These resisting forces and torques, termed inertia drag forces and torques, have the same effect as that obtained by increasing the mass and moment of inertia of the balloon. The expressions for the resulting idealized generalized inertia forces are

$$Q^I_{u_i^{(0)}} = -m_0^{(*)}\left[\ddot{u}_i^{(0)} - \dot{w}_i^{(0)}\right]$$

$$Q^I_{\theta_i^{(1)}} = -I_{ii}^{(*)}\dot{\omega}_1^{(1)} \tag{8}$$

where $Q^I_{q_i}$ is the generalized inertia drag force associated with q_i, $m_0^{(*)}$ the apparent equivalent mass ($=k\rho_a V_b$), k the constant (see Ref. 2) depending on the shape of the balloon, $I_{ii}^{(*)}$ the apparent equivalent moment of inertia with respect to the $x_i^{(1)}$ axis, and $\omega_i^{(1)} = \dot{\theta}_i^{(1)}$.

The expression for $I_i^{(*)}$ in Eq. (8) is a function of the magnitude of the balloon's radius, angular velocity, angular acceleration, and Reynolds number. Approximate values of $I_{ii}^{(*)}$ can be obtained from

$$I_{ii}^{(*)} = I_{ii}^{(a)} + I_{ii}^{(h)} \quad (i=1,2)$$

$$I_{ii}^{(a)} = \frac{\pi\rho_a D^5}{12}\left[\frac{2+\beta_i^{(a)}D}{2+2\beta_i^{(a)}D+[\beta_i^{(a)}D]^2}\right]$$

$$I_{ii}^{(h)} = \frac{\pi\rho_h D^5}{12}\left[\frac{1}{\beta_i^{(h)}D}\right]$$

$$I_{33}^{(*)} = \frac{1.94(\rho_a\mu_a)^{0.5}D^4}{|\dot{\theta}_3^{(1)}|^{0.5}} \tag{9}$$

where

D = diameter of an equivalent sphere with volume V_b
$|\dot{\theta}_3^{(1)}|$ = estimated average value of the balloon's spin velocity
μ_a = dynamic viscosity of air
ρ_h = density of helium
$\beta_i^{(a)} = [\,|\dot{\theta}_i^{(1)}|/2\nu_a\,]^{0.5}$
$\beta_i^{(h)} = [\,|\dot{\theta}_i^{(1)}|/2\nu_h\,]^{0.5}$
ν_a, ν_h = kinematic viscosity of air and helium, respectively

The expressions for the generalized forces which result from the aerodynamic viscous drag forces and torques acting on the balloon are

$$Q^D_{u_i^{(0)}} = -C_i^{(0)}\left[\dot{u}_i^{(0)} - w_i^{(0)}\right]$$

$$Q^D_{\theta_1^{(1)}} = -c^{(1)}\dot{\theta}_3^{(1)} \tag{10}$$

where $Q^D_{q_i}$ is the generalized viscous drag force associated with coordinate q_i, $C_i^{(0)}$ the equivalent translational damping coefficient, and $c^{(1)}$ the equivalent torsional damping coefficient.

The equivalent damping coefficients in Eq. (10) can be estimated from

$$C_i^{(0)} = \frac{\xi_i\rho_a}{2}A_i\,|\dot{u}_i^{(0)} - w_i^{(0)}|, \quad (i=1,2,3)$$

$$c^{(1)} = \alpha(\rho_a\mu_a)^{0.5}D^4\,|\dot{\theta}_3^{(1)}|^{0.5} \tag{11}$$

where ξ_i is the drag coefficient, $|\dot{u}_i^{(0)} - w_i^{(0)}|$ the estimated average relative velocity value, $w_i^{(0)}$ the component of wind gust velocity in the $\bar{e}_i^{(0)}$ direction, μ_a the dynamic viscosity of air, A_i the projected cross-sectional area (perpendicular to $x_i^{(0)}$), and α a constant defined in Ref. 2.

The generalized torsional forces which arise due to the torsional properties of the suspension and platform connectors have the following form:

$$Q^S_{\theta_3^{(1)}} = -k^{(2)}\left[\theta_3^{(1)} - \theta_3^{(2)}\right] - c^{(2)}\left[\dot{\theta}_3^{(1)} - \dot{\theta}_3^{(2)}\right]$$

$$Q^S_{\theta_3^{(2)}} = k^{(2)}\left[\theta_3^{(1)} - \theta_3^{(2)}\right] + k^{(3)}\left[\theta_3^{(3)} - \theta_3^{(2)}\right] + c^{(2)}\left[\dot{\theta}_3^{(1)} - \dot{\theta}_3^{(2)}\right] + c^{(3)}\left[\dot{\theta}_3^{(3)} - \dot{\theta}_3^{(2)}\right]$$

$$Q^S_{\theta_3^{(3)}} = k^{(3)}\left[\theta_3^{(2)} - \theta_3^{(3)}\right] + c^{(3)}\left[\dot{\theta}_3^{(2)} - \dot{\theta}_3^{(3)}\right] \tag{12}$$

where Q^S_{qi} is the generalized force due to torsional properties of the suspension system. $k^{(2)}$ the equivalent torsional stiffness of the suspension connector, $c^{(2)}$ the equivalent torsional damping coefficient for the suspension connector, $k^{(3)}$ the equivalent torsional stiffness of the platform connector, and $c^{(3)}$ the torsional damping of the platform connector.

Generalized Math Model

The form of the generalized math model is obtained by substituting the expressions from Eqs. (5-12) into Lagrange's equation (4). The resulting expression for the generalized force Q_i is obtained by summing the corresponding contributions from Eqs. (7-12). The final form of the model is as

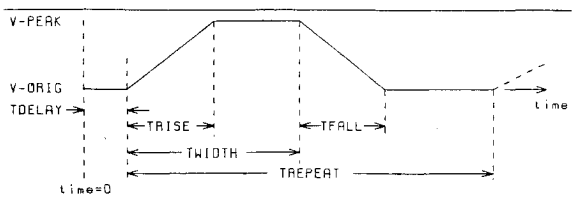

VARIABLE	CASE 1	CASE 2
VORIG	0.0 m/sec	0.0 m/sec
VPEAK	1.52 x 10^{-3}m/s	1.52 x 10^{-3}m/s
TDELAY	0.0 sec	0.0 sec
TRISE	1.5 sec	1.0 sec
TWIDTH	6.0 sec	6.0 sec
TFALL	1.0 sec	1.05 sec
TREPEAT	25.05 sec	15.0 sec

Fig. 5 Pulse form of wind gust velocity.

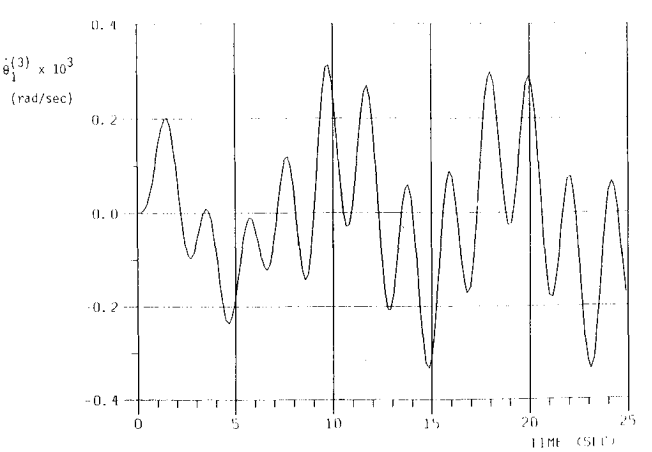

Fig. 6 Platform angular velocity vs time (case 1).

follows:

$$M_i\ddot{\bar{q}}_i + C_i\dot{\bar{q}}_i + K_i\bar{q}_i = \bar{F}_i \quad (i=1,2,3)$$

where

$$\bar{q}_i = (u_i^{(0)},\ \theta_i^{(1)}\ \theta_i^{(2)}\ \theta_i^{(3)})^T$$

$M_i =$

$$\begin{bmatrix} [m_0^{(*)}+\sigma_0] & [(-1)^i\ r_1\sigma_1] & [(-1)^i\ r_2\sigma_2] & [(-1)^i\ r_3\sigma_3] \\ [(-1)^i r_1\sigma_1] & [(I_{ii}^{(*)}+I_{ii}^{(0)}+r_i^2\sigma_1)] & [(r_1r_2\sigma_2)] & [(r_1r_3\sigma_3)] \\ [(-1)^i r_2\sigma_2] & [(r_2r_1\sigma_1)] & [(r_2^2\sigma_2)] & [(r_2r_3\sigma_3)] \\ [(-1)^i r_3\sigma_3] & [(r_3r_1\sigma_3)] & [(r_3r_2\sigma_3)] & [(I_{ii}^{(3)}+r_3^2\sigma_3)] \end{bmatrix}$$

$$M_3 = \begin{bmatrix} [m_0^{(*)}+\sigma_0] & 0 & 0 & 0 \\ 0 & [(I_{33}^{(*)}+I_{33}^{(0)}] & 0 & 0 \\ 0 & 0 & [I_{33}^{(2)}] & 0 \\ 0 & 0 & 0 & I_{33}^{(3)} \end{bmatrix}$$

$$\sigma_i = \sum_{k=i}^{3} m_k$$

$$C_i = \begin{bmatrix} [C_i^{(0)}] & 0\ 0\ 0 \\ 0 & 0\ 0\ 0 \\ 0 & 0\ 0\ 0 \\ 0 & 0\ 0\ 0 \end{bmatrix}$$

$$C_3 = \begin{bmatrix} C_3^{(0)} & 0 & 0 & 0 \\ 0 & [c^{(1)}+c^{(2)}] & -c^{(2)} & 0 \\ 0 & -c^{(2)} & [c^{(2)}+c^{(3)}] & -c^{(3)} \\ 0 & 0 & -c^{(3)} & c^{(3)} \end{bmatrix}$$

$$K_i = \begin{bmatrix} 0 & 0 & 0 & 0 & 0 \\ 0 & [(r_1\sigma_1-\epsilon_3\sigma_0)g] & 0 & 0 & 0 \\ 0 & 0 & [r_2\sigma_2 g] & 0 & 0 \\ 0 & 0 & 0 & 0 & [r_3\sigma_3 g] \end{bmatrix}$$

$$K_3 = \begin{bmatrix} K^{(0)} & 0 & 0 & 0 \\ 0 & k^{(2)} & -k^{(2)} & 0 \\ 0 & -k^{(2)} & [k^{(2)}+k^{(3)}] & -k^{(3)} \\ 0 & 0 & -k^{(3)} & k^{(3)} \end{bmatrix}$$

$$\bar{F}_1 = \begin{bmatrix} [\rho_a V_b + m_0^{(*)}]\,\dot{w}_1^{(0)} + C_1^{(0)} w_1^{(0)} \\ \rho_a V_b \epsilon_3 \dot{w}_2^{(0)} \\ 0 \\ 0 \end{bmatrix}$$

$$\bar{F}_2 = \begin{bmatrix} [\rho_a V_b + m_0^{(*)}]\,\dot{w}_2^{(0)} + C_2^{(0)} w_2^{(0)} \\ -\rho_a V_b \epsilon_3 \dot{w}_1^{(0)} \\ 0 \\ 0 \end{bmatrix}$$

$$\bar{F}_3 = \begin{bmatrix} [\rho_a V_b + m_0^{(*)}]\,\dot{w}_3^{(0)} + C_3^{(0)} w_3^{(0)} \\ \rho_a V_b (\epsilon_1 \dot{w}_2^{(0)} - \epsilon_2 \dot{w}_1^{(0)}) \\ 0 \\ 0 \end{bmatrix} \tag{13}$$

A close inspection of Eq. (13) reveals that the general motion of the idealized balloon system is comprised of the following uncoupled motions: 1) translation and pendulation in the plane of the $x_1^{(3)}x_3^{(3)}$ body axis, 2) translation and pendulation motion in the $x_2^{(3)}x_3^{(3)}$ plane, 3) spin motion about the $x_3^{(3)}$ axis, and 4) bounce in the direction of the $x_3^{(3)}$ axis. Note that the two planar motion models ($i=1,2$) are identical in form.

Although the various models are uncoupled, the spin model must be solved first (unless $\epsilon_1=\epsilon_2=0$) since the components of $w_i^{(0)}$ and $\dot{w}_i^{(0)}$ in Eq. (13) are rewritten as

$$\begin{aligned} w_1^{(0)} &= W_1\cos\theta_3^{(3)} + W_2\sin\theta_3^{(3)} \\ w_2^{(0)} &= W_1\sin\theta_3^{(3)} + W_2\cos\theta_3^{(3)} \\ w_3^{(0)} &= W_3 \\ \dot{w}_1^{(0)} &= \dot{W}_1\cos\theta_3^{(3)} + \dot{W}_2\sin\theta_3^{(3)} \\ \dot{w}_2^{(0)} &= \dot{W}_1\sin\theta_3^{(3)} + \dot{W}_2\cos\theta_3^{(3)} \\ \dot{w}_3^{(0)} &= \dot{W}_3 \end{aligned} \tag{14}$$

where W_i, $\dot{W}_i$ $(i=1,2,3)$ are components of the wind gust velocity and acceleration along the inertial reference axis.

Equation (14) was developed by assuming small values for W_1, W_2, W_3, $\theta_1^{(3)}$, $\theta_2^{(3)}$, $\theta_3^{(3)}$. The values of $\theta_3^{(3)}$ (and hence $w_1^{(0)}$) are obtained by first solving the spin model and then substituting these into the pendulation model.

The general motion of the balloon system is obtained by solving Eq. (13) on the digital computer. For this purpose, the math model is rewritten in state variable form as

$$\dot{\bar{\zeta}}_i = A_i\bar{\zeta}_i + \bar{P}_i \quad (i=1,2,3)$$

where

$$A_i = \begin{bmatrix} 0 & I \\ -M_i^{-1}K_i & -M_i^{-1}C_i \end{bmatrix} \qquad \bar{P}_i = \begin{bmatrix} \bar{0} \\ M_i^{-1}\bar{F}_i \end{bmatrix}$$

$$\bar{\zeta}_i = (\bar{q}_i^T, \dot{\bar{q}}^T)^T \tag{15}$$

where $\bar{0}$ is the null vector and I the identity matrix.

Table 1 Properties of the idealized LACATE system

$C_1^{(0)} = C_2^{(0)} = C_3^{(0)} = 0.0$ lb·s/ft	$m_2 = 4.20$ slug (61.2 kg)
$c^{(1)} = 0.0$ lb·s/ft	$m_3 = 11.66$ slug (170 kg)
$c^{(2)} = c^{(3)} = 0.0$ lb·s/ft	$m_0^{(*)} = 154.0$ slug (2.25×10^3 kg)
$D = 420$ ft (128 m)	$r_1 = 222$ ft (67.7 m)
g = 31.7 ft/s^2 (9.66 m/s^2)	$r_2 = 75$ ft (22.9 m)
$I_{11}^{(1)} = I_{22}^{(1)} = 1.57 \times 10^6$ slug ·ft^2 (2.13×10^6 kg·m^2)	$r_3 = 15$ ft (4.57 m)
$I_{11}^{(*)} = I_{22}^{(*)} = 0.064 \times 10^6$ slug ·ft^2 (0.087×10^6 kg·m^2)	$V_b = 39.0 \times 10^6$ ft^3 (1.104×10^6 m^3)
$I_{33}^{(1)} = 2.12 \times 10^6$ slug ·ft^2 (2.87×10^6 kg·m^2)	$\alpha = 0.16$
$I_{33}^{(*)} = 2.44 \times 10^6$ slug ·ft^2 (3.31×10^6 kg·m^2)	$\epsilon_1 = \epsilon_2 = 0.0$ ft (0.0 m)
$I_{11}^{(3)} = I_{22}^{(3)} = 0.0$ slug ·ft^2 (0.0 kg·m^2)	$\epsilon_3 = 23.7$ ft (7.22 m)
$I_{33}^{(3)} = 6.0$ slug ·ft^2 (8.13 kg·m^2)	$\mu_a = 3.6 \times 10^{-7}$ slug/ft·s (1.72×10^{-5} kg/m·s)
$k^{(2)} = 250$ lb/ft (3650 N/m)	$\mu_h = 3.5 \times 10^{-7}$ slug/ft·s (1.68×10^{-5} kg/m·s)
$K^{(0)} = 0.12$ lb/ft (1.75 N/m)	$\rho_a = 7.9 \times 10^{-6}$ slug/ft^3 (4.07×10^{-3} kg/m^3)
$m_0 = 103.7$ slug (1.51×10^3 kg)	$\rho_h = 3.6 \times 10^{-7}$ slug/ft^3 (1.86×10^{-4} kg/m^3)
$m_1 = 4.20$ slug (61.2 kg)	

Table 2 Results from modal analysis

i	Frequency Ω_i rad/s	Period τ_i, s	Eigenvector $\bar{x}_i$
1	0	—	$\begin{bmatrix} 1 \\ 0 \\ 0 \\ 0 \end{bmatrix}$
2	0.14	46.1	$\begin{bmatrix} 1.0 \\ 0.60 \times 10^{-1} \\ 0.76 \times 10^{-2} \\ 0.76 \times 10^{-2} \end{bmatrix}$
3	0.74	8.51	$\begin{bmatrix} 1.0 \\ -0.37 \times 10^{-1} \\ 0.35 \\ 0.34 \end{bmatrix}$
4	3.04	2.07	$\begin{bmatrix} 1.0 \\ -0.35 \times 10^{-1} \\ 5.2 \\ -34.37 \end{bmatrix}$

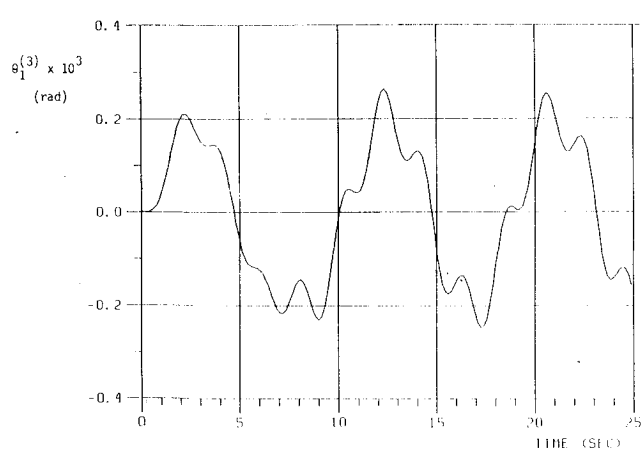

Fig. 7 Platform angular displacement vs time (case 1).

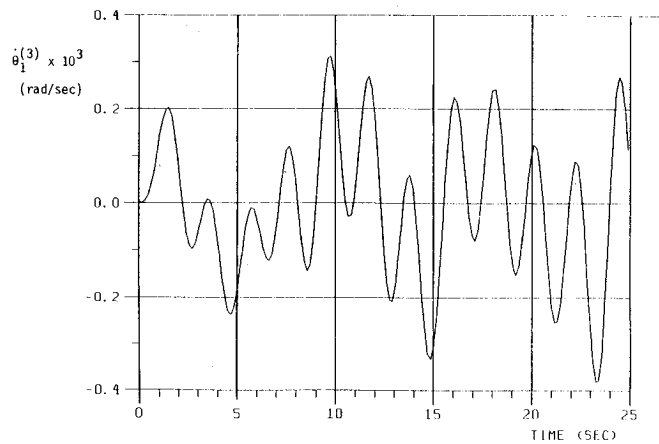

Fig. 8 Platform angular velocity vs time (case 2).

There are many instances in which it is desirable to determine the natural frequencies and modal shapes of the balloon system. The following simplified form of Eq. (13) is used for this purpose:

$$M_i \ddot{\bar{q}}_i + K_i \bar{q}_i = \bar{0} \tag{16}$$

The system natural frequencies and corresponding modal shapes are obtained by solving the eigenvalue problem resulting from Eq. (16); this is given as

$$(K_i - \Omega^2 M_i)\bar{X} = \bar{0} \qquad (i = 1,2,3) \tag{17}$$

where $\Omega_1 \ldots \Omega_{N_i}$ are the system natural frequencies, $\bar{X}_1 \ldots \bar{X}_{N_i}$ the eigenvectors defining the modal shapes, and N_i the order of the M_i and K_i matrices.

Results

The math model developed in this study was used to simulate the motion of the LACATE balloon system shown in Fig. 1 and the results were compared with actual flight data in order to obtain some indication of the validity of the model. The LACATE system was employed in an experiment by NASA engineers in order to sense remote vertical profiles of temperature and the concentration of selected atmospheric trace constituents. The system was launched from White Sands Missile Range in May 1974 and consisted of a 39.0×10^6 ft^3 (1.104×10^6 m^3) zero pressure balloon, a

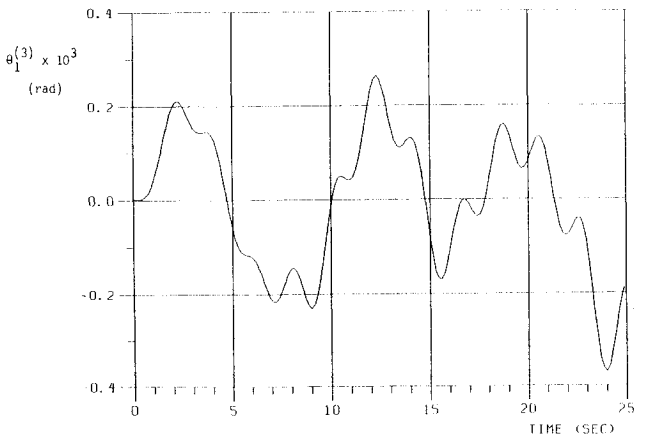

Fig. 9 Platform angular displacement vs time (case 2).

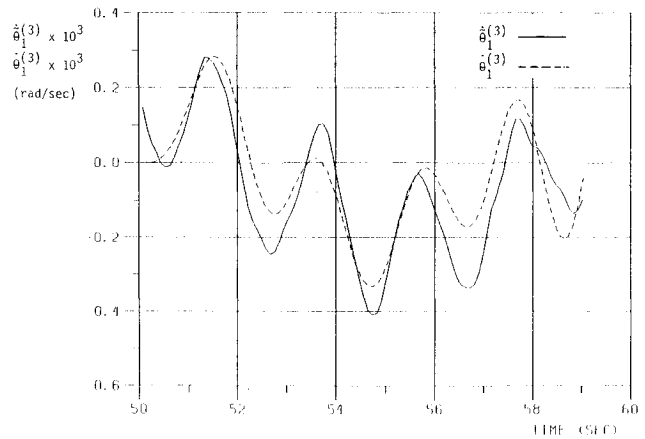

Fig. 10 Comparison of predicted and actual velocity (1).

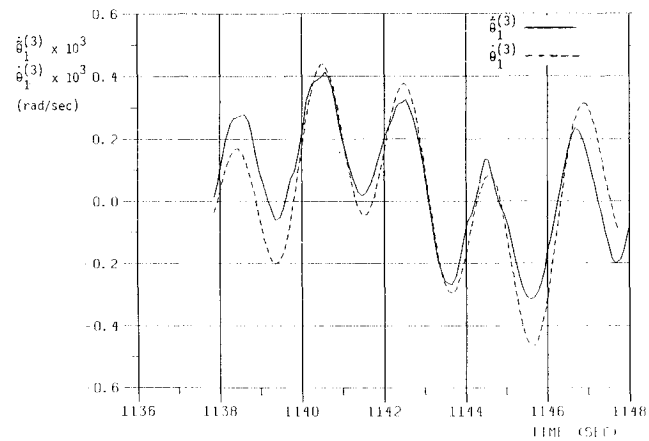

Fig. 11 Comparison of predicted and actual velocity (2).

recovery AFCRL parachute, flight control electronics, and an observational (research) platform. The observational platform housed a 10 channel radiometer, 3 orthogonally oriented rate gyros, 2 magnetometers, temperature and water vapor pressure sensors, transmitters, and batteries. The platform, suspension system, and balloon were connected by ring- and clevis-connectors.

The LACATE balloon system was designed to attain a float altitude of 130,000 ft (40,000 m) at 32.6°N latitude and 106°W longitude. Data from the gyros and magnetometers were recorded continuously and telemetered back to ground

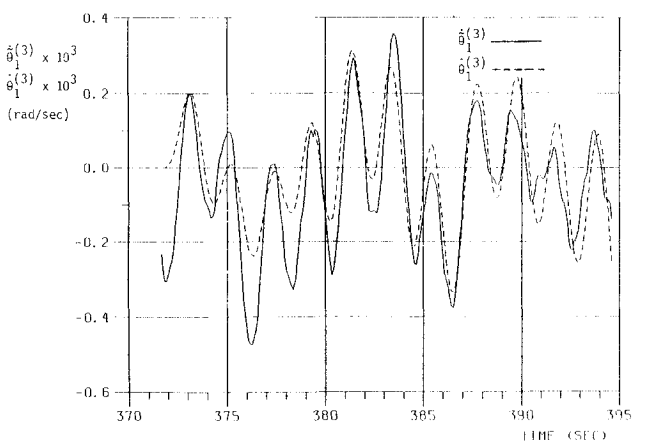

Fig. 12 Comparison of predicted and actual velocity (3).

control after the system reached float altitude. Additional data on the balloon's horizontal and vertical trajectory components were obtained from a radar tracking installation. The data recording process was continued over a period of approximately 5 h beginning at 5 h, 5 min, 20 s Mountain daylight time. The line cutter was activated at the end of the experiment and the platform returned to ground via the parachute.

For simulation purposes, the Lacate system was idealized as one comprised of three links (i.e., balloon, research platform, and one link suspension system) as shown in Fig. 2. This idealization was based on the number and location of the ring-and-clevis connectors (see Fig. 1). Properties of the idealized balloon system are presented in Table 1. These properties were used to compute the values of $m_0^{(*)}$, $I_{ii}^{(*)}$etc., which are also given in Table 1. The magnitudes of the values of ϵ_1, ϵ_2, $k^{(2)}$, $c^{(2)}$, $k^{(3)}$ and $c^{(3)}$ were not available and hence these were based (when possible) on results from actual flight data. It is of interest to note that the values of $m_0^{(*)}$ and $I_{33}^{(*)}$ are significant in comparison to the respective values of m_0 and $I_{33}^{(1)}$ while the values of $I_{11}^{(*)}$ and $I_{22}^{(*)}$ are negligible in comparison to $I_{11}^{(1)}$ and $I_{22}^{(1)}$.

The natural system frequencies and modal shape functions for the pendulation model ($i=1,2$) were obtained by solving Eq. (17) on the computer and the results are presented in Table 2. The shape functions are plotted in Fig. 4 for ease of interpretation. The results in Table 2 and Fig. 4 indicate the following:

1) The first (zero frequency) mode consists of a pure translation of the entire system.

2) The second mode consists primarily of a pendulation oscillation of the balloon.

3) The third mode consists primarily of an in-phase pendulation oscillation of the suspension links and research platform.

4) The fourth mode consists primarily of a pendulation oscillation of the platform.

The pendulation motion of the LACATE balloon system due to the effect of the wind gusts was simulated by employing a numerical algorithm and solving Eq. (15) on the digital computer. Typical results for the pendulation angle $\theta_1^{(3)}$ and angular velocity $\dot{\theta}_1^{(3)}$ are plotted in Figs. 6-9. These results were obtained by assuming a wind gust velocity form recommended by NASA engineers, See Fig. 5.

A close inspection of Figs. 6-9 reveals that the wind gust input excites (primarily) the third and fourth normal modes of the system. As expected, the contribution of the fourth normal mode is less significant in the integrated $\dot{\theta}_1^{(3)}$ (i.e., $\theta_1^{(3)}$) curve. Moreover, the maximum value of $\theta_1^{(3)}$ is extremely small; i.e., less than 0.02 deg. Clearly, this is a function of the magnitudes of V_{peak} and T_{rise} selected in this study. The behavior was also observed for other pulse forms

of wind gust inputs with different values of V_{peak} and T_{rise}. This type of behavior is similar to that reported by others who have investigated the wind gust response of buoyant vehicles with slung loads.[9-12]

Results for the platform angular velocity due to the wind gust input were compared with actual gyro data furnished by NASA in order to obtain some verification of the system pendulation model. The pulse form of the wind gust shown in Fig. 5 was again employed for this purpose; however, the magnitudes of the input parameters were systematically adjusted until an optimal fit was obtained. Typical comparisons of results for $\dot{\theta}_i^{(3)}$ are shown in Figs. 10-12. The agreement of these fits indicates that the system pendulation model presented in this paper yields very realistic results. The agreement can be improved further by adjusting the model input and/or characteristic parameters. This can be accomplished by employing the parameter estimation methods discussed in Refs. 4-6.

The torsional model [Eq. (13), $i=3$] developed in this study is a generalization of torsional models reported in Ref. 13. The evaluation of this model will be a topic for future research.

Acknowledgment

This work was supported (in part) by the National Aeronautics and Space Administration under Grant NAGL-65. The author is grateful to Ms. Jean Menzner for her patience in typing this manuscript.

References

[1]Harwitt, M., "Infrared Astronomy and the Shuttle," *Astronautics and Aeronautics,* Vol. 12, Oct. 1974, pp. 23-28.

[2]Nigro, N. J., Elkouh, A. F., Shen, K. S., Nimityongskul, P., Jhaveri, V. N., and Sethi, A., "Attitude Determination of a High Altitude Balloon System: Part I. Development of the Mathematical Model," NASA CR 142193, 1975.

[3]Nigro, N. J., Elkouh, A. F., "Attitude Determination of the LACATE Balloon System," *Proceedings of Ninth AFGL Scientific Balloon Symposium,* Vol. 20, Aug. 1967, pp. 239-262.

[4]Nigro, N. J., Elkouh, A. E., Shen, K. S., Nimityongskul, P., Jhaveri, V. N., and Sethi, A., "Attitude Determination of a High Altitude Balloon System: Part II. Development of the Parameter Determination Process," NASA CR 145958, 1976.

[5]Nigro, N. J., Nimityongskul, P., and Hinton, D. E., "Improved Method for Predicting Attitude of Balloon Gondolas," *Proceedings of Tenth AFGL Scientific Balloon Symposium,* Vol. 21, Aug. 1978, pp. 433-460.

[6]Nigro, N. J. and Gagliardi, J. C., "Feasibility of Observer Systems for Determining Attitude of Balloon Borne Research Platforms," NASA CR 168945, 1982.

[7]Nigro, N. J. and Johanek, F. M., "Effect of Wind Gusts on Motion of Balloon Borne Research Platforms," NASA CR 168947, 1982.

[8]Nigro, N. J., Yang, Jen-Kang, "Computer Program for Balloon System Simulation," NASA CR 172451, 1984.

[9]Tischler, M. B., Jex, H. R., and Ringland, R. F., "Simulation of Heavy-Lift Airship Dynamics Over Large Ranges of Speed and Incidence," AIAA Lighter-Than-Air Systems Technology Conference, Annapolis, MD, July 1981, pp. 96-115.

[10]Tischler, M. B., Ringland, R. F., and Jex, H. R., "Flight Dynamics Analysis and Simulation of Heavy-Lift Airships, Vol. II, Technical Manual," NASA CR 166471, Dec. 1982.

[11]Tischler, M. B., Ringland, R. F., and Jex, H. R., "Heavy-Lift Airship Dynamics," *Journal of Aircraft,* Vol. 20, May 1983, pp. 425-433.

[12]Tischler, M. B. and Jex, H. R., "Effects of Atmospheric Turbulence on a Quadrotor Heavy Lift Airship," *Journal of Aircraft,* Vol. 20, Dec. 1983, pp. 1050-1057.

[13]Morris, A. L. and Stefan, K. H., "High Attitude Balloon as Scientific Platforms," Technical Report No. 2, National Center for Atmosphere Research, Boulder, CO, Jan. 1969.